JACS
JOURNAL OF THE AMERICAN CHEMICAL SOCIETY
Article
pubs.acs.org/JACS

Dynamics in the Interior of AOT Lamellae Investigated with Two-Dimensional Infrared Spectroscopy

S. K. Karthick Kumar, A. Tamimi, and Michael D. Fayer*

Department of Chemistry, Stanford University, Stanford, California 94305, United States

ABSTRACT: The dynamics inside the organic regions of aerosol-OT (AOT)/water mixtures in the lamellar mesophase, bicontinuous cubic (BC) phase, and in an analogous molecule without the charged sulfonate headgroup are investigated by observing spectral diffusion, orientational relaxation and population relaxation using ultrafast two-dimensional infrared (2D IR) vibrational echo spectroscopy and IR pump−probe experiments on the asymmetric CO stretch of a vibrational probe, tungsten hexacarbonyl ($W(CO)_6$). The water layer thickness between the bilayer planes in the lamellar phase was varied. For comparison, the dynamics of $W(CO)_6$ in the normal liquid bis(2-ethylhexyl) succinate (EHS), which is analogous to AOT but has no charged sulfonate headgroup, were also studied. The 2D IR experiments measure spectral diffusion, which results from the structural evolution of the system. Spectral diffusion is quantified by the frequency−frequency correlation function (FFCF). In addition to a homogeneous component, the FFCFs are biexponential decays with fast and slow time components of ∼12.5 and ∼150 ps in the lamellar phase. Both components of the FFCF are independent of the number of water molecules per headgroup for the lamellae, but they slow somewhat in the BC phase. The dynamics in the ordered phases are in sharp contrast to the dynamics in EHS, which displays fast and slow components of the FFCF of 5 and 80 ps, respectively. As the hydration level of AOT increases, vibrational lifetime decreases, suggesting some change in the local environment of $W(CO)_6$ with water content.

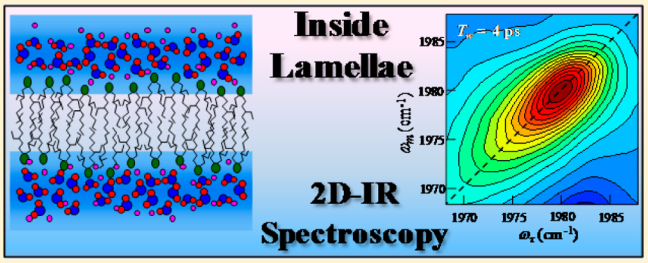

1. INTRODUCTION

Mesomorphic phases appear in many surfactant systems and with increasing surfactant concentration. For example, the surfactant AOT (aerosol-OT, sodium bis(2-ethylhexyl) sulfosuccinate) in mixtures with water with increasing AOT concentration at room temperature goes through the phases: isotropic, lamellar, bicontinuous cubic (BC), and inverse hexagonal.[1] The lamellar structure occurring in surfactant systems has been shown by a variety of techniques as being composed of macroscopically extended bilayers of amphiphilic molecules alternating with water layers.[2,3] Lyotropic lamellar phases are important as models of logical membranes[4−6] and in various scientific and technological applications.[7,8] Biological membranes have a basic bilayer structure. In addition to a permeability barrier, the plasma membrane serves as the "solvent" for membrane proteins and other biological molecules. Therefore, the nature of the internal dynamics of lamellar structures (bilayers) is important for understanding processes that occur within them.[9−13] The BC phase has an interesting thermodynamically stable structure consisting of what is essentially a branching network of surfactant cylinders in three dimensions with congruent networks of water channels.[14,15] It has been suggested that the BC phase is an intermediate between the inverted hexagonal phase (parallel cylinders) and the lamellar phase.

AOT gives rise to lamellar structures when mixed with water in a wide range of AOT/water ratios. At room temperature, the AOT lamellar phase occurs in the range from ∼12 to ∼78 wt% AOT.[1] The lamellar repeat distances have been characterized by X-ray diffraction and scale linearly with the reciprocal of the AOT volume fraction.[3,16,17] The structure of AOT is shown in Figure 1A. It contains a sulfonate headgroup and a sodium counterion that preferentially partition into the water phase. There are ester moieties near the headgroup that may also interact with the water as well as the sodium counterion depending on the packing and configuration of the AOT molecules.[18−21] The alkyl chains are branched and bulky and their steric interactions with one another play an important role in determining the surface area per AOT molecule in lamellar phases and in reverse micelles.[3,18,22] Various studies have been carried out to investigate the hydration of lipid membranes,[5,23−25] and experiments and simulations have shown that water molecules penetrate the interfacial region of bilayers to some extent, but have a low probability of being found in the hydrophobic core.[19,26−28] Dynamical studies of the AOT/water system in the lamellar phase have been somewhat sparse. Some of these studies have focused on water diffusion[29−31] while others have explored the effect of water/surface interactions and confinement geometry on the dynamics of the water.[18,32] X-ray, NMR, and fluorescence experiments have also been used to study the model membranes mainly to study the effect of cholesterol on the depth of water penetration.[33−37]

Received: December 28, 2012

 © XXXX American Chemical Society dx.doi.org/10.1021/ja312676e | J. Am. Chem. Soc. XXXX, XXX, XXX−XXX

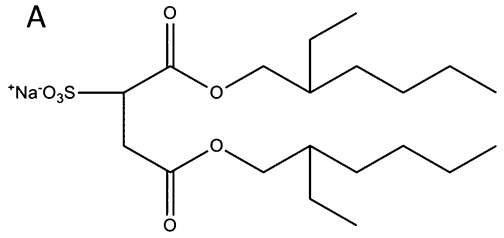

AOT (aerosol-OT, sodium bis(2-ethylhexyl) sulfosuccinate)

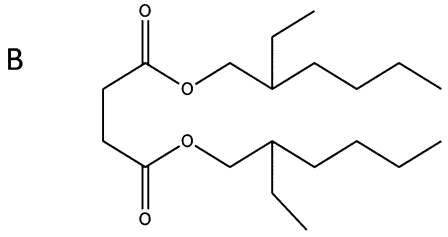

bis(2-ethylhexyl) succinate

Figure 1. Structures of (A) AOT (aerosol-OT, sodium bis(2-ethylhexyl) sulfosuccinate) and (B) bis(2-ethylhexyl) succinate (EHS).

In this paper we investigate the internal dynamics of AOT lamellar structures, the BC phase, and a related model compound. Measurements of spectral diffusion, orientational relaxation, and population relaxation were made using two-dimensional infrared (2D IR) vibrational echo spectroscopy and pump probe experiments. The experiments were performed on a vibrational dynamics probe molecule, the triply degenerate asymmetric CO stretching mode of tungsten hexacarbonyl ($W(CO)_6$) at room temperature. $W(CO)_6$ is completely insoluble in water and therefore resides in the hydrophobic interior of the AOT lamellar and BC structures. The number of water molecules per surfactant is given by the parameter $\lambda = [H_2O]/[AOT]$. The lamellar phase was studied over a wide range of hydration levels from $\lambda = 98$ to 16. The BC phase only occurs in a very narrow range of hydration, and measurements were made with $\lambda = 6$.

To investigate the effect of structural ordering in the mesophases on their dynamics, the same experiments were performed on $W(CO)_6$ in a disordered liquid that is chemically equivalent to the interior of the AOT lamellar and BC structures. The model system is the room temperature liquid bis(2-ethylhexyl) succinate (EHS, $C_{20}H_{38}O_4$), which has the same chemical structure as AOT but without the charged sulfonate headgroup. The structure of EHS is shown in Figure 1B.

Recently, using ultrafast infrared spectroscopy, dynamics of water between the bilayers in AOT lamellar structures and in the water nanopools in AOT spherical reverse micelles were probed.[18,38−42] The experiments investigated the influence of interactions with the AOT interface on the dynamics of water. The experiments compared water dynamics in the planar lamellar geometry and the spherical reverse micelle geometry as a function of the number of water molecules per AOT headgroup. In contrast to those experiments on water, the current experiments examine the dynamics in the surfactant interiors in the lamellar and BC mesophases.

The 2D IR experiments measure spectral diffusion, which is the time evolution of the vibrational frequencies of the probe molecule vibration within the inhomogeneously broadened absorption line. Spectral diffusion is the result of the structural evolution of the system that causes the local environments of the probe molecules to change, which in turn changes the probe vibrational frequency. Therefore, spectral diffusion reports on the time dependence of the structural evolution of the system. The 2D IR measurements of spectral diffusion yield the frequency−frequency correlation function (FFCF), which quantifies the dynamic time scales and amplitudes of contributions to the structural changes in the system.[43−47] The polarization-selective IR pump−probe experiments measure the vibrational lifetime and orientational relaxation. The vibrational lifetime is very sensitive to the local environment. Changes in local environment of the vibrational probe can result in changes in the lifetime.

The FFCFs obtained from the 2D IR experiments yield a homogeneous (ultrafast structural fluctuations) component and two spectral diffusion components. In the lamellar phase, the spectral diffusion components are independent of the number of water molecules per headgroup (λ) within experimental error, and have fast and slow component values of ∼12.5 and ∼150 ps, respectively. When the amount of water is reduced, the phase changes to BC, and both components of the spectral diffusion slow (∼15 and ∼180 ps), showing that the dynamics are sensitive to the structural phase but not sensitive to the amount of water so long as the system remains in the lamellar phase. In contrast to these ordered phases, the two components of the spectral diffusion in the EHS disordered liquid model of AOT are ∼5 and ∼80 ps, which shows that the mesophase structure has a substantial impact on the internal dynamics of the lamellar and BC phases. Although the spectral diffusion does not change with λ (number of water molecules between bilayers) in the lamellar phase, the vibrational lifetime does change to some extent, indicating a local change in the environment of the vibrational probe.

2. EXPERIMENTAL PROCEDURES

Succinic anhydride, 2-ethyl-1-hexanol, toluene, and *p*-toluenesulfonic acid (Sigma-Aldrich) were used as received. Aerosol-OT (AOT, sodium bis(2-ethylhexyl) sulfosuccinate) (Sigma-Aldrich) was purified by dissolving the compound in methanol and stirring overnight with activated charcoal. The charcoal was removed by vacuum filtration, and methanol was removed by rotary evaporation.

Bis(2-ethylhexyl) succinate (EHS), the model compound, was synthesized and purified following a related procedure for the synthesis of a variant of AOT[48] as follows: 10 g of succinic anhydride and 21 g of 2-ethyl-1-hexanol were dissolved in 250 mL of toluene, and 2.2 g of *p*-toluenesulfonic acid were added as a catalyst. The reaction mixture was heated to 120 °C for 15 h in a round-bottom flask with an attached Dean−Stark water-trap. The reaction mixture was subsequently washed a few times with aqueous $NaHCO_3$ solution. The organic phase was dried over $MgSO_4$, and the solvent was removed using a rotary evaporator. The mixture was then purified using flash column chromatography over silica with a 10−20% EtO_2/petroleum ether solvent gradient.

Tungsten hexacarbonyl was dissolved in methylene chloride and added to the surfactant or EHS, such that the ratio of probe molecule to surfactant or to EHS was 1:600. In the surfactant systems, water was added after slow evaporation of methylene chloride overnight. AOT/water mixtures were made with AOT weight percentages 20, 30, 40, 50, 60, and 80, which correspond to water to surfactant ratios $\lambda = 98$, 57, 37, 24, 16, and 6. The water thickness of lamellar samples of varying water to surfactant ratios has been determined by X-ray diffraction.[3,16,17] Samples for FT-IR absorption experiments and 2D IR and IR pump−probe experiments were housed in sample cells with CaF_2 windows separated by 12 μm Teflon spacers.

dx.doi.org/10.1021/ja312676e | J. Am. Chem. Soc. XXXX, XXX, XXX−XXX

A Ti:sapphire oscillator/regenerative amplifier with a repetition rate of 1 kHz, which produced 100 fs pulses with pulse energies of ~700 μJ and a wavelength centered at 800 nm, was used to pump a home-built mid-IR optical parametric amplifier to generate ~170 fs pulses centered at 1980 cm^{-1} with ~5 μJ pulse energy. The mid-IR pulses were then co-aligned with a He−Ne beam and a 90:10 ZnSe beam-splitter was used to split the incoming pulse into a weaker probe pulse and a stronger pump pulse. The weak pulse is routed through a mechanical delay line which is used to set the waiting time T_w (see below). The strong pulse was sent to a mid-IR Fourier-domain pulse-shaper. Details of the laser system and the pulse shaper have been presented.[49] The output beam from the pulse shaper, which generated pulses 1 and 2 in the vibrational echo experiments, is focused into the sample using a 150 mm focal length CaF_2 lens and the weak probe pulse (pulse 3) is focused in the sample using a 100 mm focal length CaF_2 lens to give spot size diameters of ~250 and ~180 μm, respectively. The probe is collimated after the sample then sent to a spectrometer equipped with a 32-element HgCdTe IR array detector.

In a 2D IR vibrational echo experiment, τ (the time between pulses 1 and 2) is scanned for a fixed T_w (the time between pulse 2 and 3), and a 2D spectrum is obtained by Fourier transforming along the τ dimension. Then T_w is changed, and τ is scanned to obtain another 2D spectrum. A series of such spectra is recorded. The desired information is contained in the peak positions and the T_w dependence of the amplitudes and shapes of the peaks in the 2D spectrum. In the pump−probe experiments, two pulses, a strong pump and a weak probe, impinge on the sample. The time between the two pulses is t. The pump produces a transient change in the transmission of the probe. The probe is frequency resolved by the spectrograph, and its amplitude at each frequency is measured as a function of t. The change in probe transmission is obtained with the pump polarization parallel to the probe and at the magic angle of 54.7°.

The FFCF, which quantifies the spectral diffusion in terms of the amplitudes and time scales of the dynamics, is the joint probability that a vibration with an initial (t = 0) frequency in the inhomogeneous spectral distribution will maintain its frequency at a later time t, averaged over all initial frequencies. To extract the FFCF from the 2D spectra, center line slope (CLS) analysis was employed.[46,47]

The FFCF is described with a multiexponential model,

$$C_1(t) = \langle \delta\omega_{1,0}(t)\delta\omega_{1,0}(0)\rangle = \sum_i \Delta_i^2 \exp(-t/\tau_i) \quad (1)$$

where the Δ_i are the frequency fluctuation amplitudes of each component, and the τ_i are their associated time constants. A component of the FFCF with $\Delta\tau < 1$ is motionally narrowed, and it is the dominant source of the homogeneous broadening of the absorption line. When a component is motionally narrowed, Δ and τ cannot be determined separately. The motionally narrowed homogeneous contribution to the absorption spectrum has a pure dephasing line width given by $\Gamma^* = \Delta^2\tau = 1/\pi T_2^*$, where T_2^* is the pure dephasing time. The observed homogeneous dephasing time, T_2, also has contributions from the vibrational lifetime and orientational relaxation:

$$\frac{1}{T_2} = \frac{1}{T_2^*} + \frac{1}{2T_1} + \frac{1}{3T_{or}} \quad (2)$$

where T_2^*, T_1, and T_{or} are the pure dephasing time, vibrational lifetime, and orientational relaxation times, respectively. The total homogeneous line width is $\Gamma = 1/\pi T_2$.

CLS analysis of the T_w-dependent 2D IR line shapes permits the FFCF to be determined in the following manner.[46,47] The 2D spectrum at a given T_w is sliced parallel to the ω_m axis (the vertical axis in the 2D spectra) over a range of frequencies about the center of the spectrum. Each slice is fit to a Gaussian line shape function to obtain its peak position. The peak positions are plotted against the corresponding ω_τ frequencies of the slices. (ω_τ is the horizontal axis in the 2D spectra.) The set of peak positions (ω_τ,ω_m) are referred to as center line data, and the resulting line is fit with a linear regression to obtain its slope. Slopes are obtained for each T_w and plotted. The slopes can range from 1 to 0. A fit to the CLS vs T_w curve gives the spectral diffusion time constants and amplitude factors. The difference between the T_w = 0 intercept of the CLS plot and 1 is related to the homogeneous component of the FFCF. To obtain homogeneous component, the CLS fitting results are used to simultaneously fit the FT-IR absorption spectrum and the CLS data.[46,47] The homogeneous component is included in the full FFCF.

The polarization selective pump−probe technique tracks the decay of the probe transmission with polarizations parallel ($I_\parallel$) and at the magic angle (MA = 54.7°) relative to the pump pulse polarization. The data contain information about both population and orientational dynamics.

$$I_\parallel = P(t)(1 + 0.8C_2(t)) \quad (3)$$

$$I_{MA} = P(t) \quad (4)$$

$P(t)$ is the vibrational population relaxation and $C_2(t)$ is the second Legendre polynomial correlation function, which is the orientational correlation function for the vibrational mode. Measurements of I_{MA} enable $C_2(t)$ to be extracted from measurements of $I_\parallel$. Here $C_2(t)$ is a single-exponential decay characterized by the orientational relaxation time, τ_r.

3. RESULTS AND DISCUSSION

3.1. FT-IR Absorption Spectra. $W(CO)_6$ is used as a vibrational spectral probe of dynamics and structure. $W(CO)_6$ is substantially smaller than AOT. It has a molecular volume of ~95 $Å^3$, compared to the molecular volume of AOT, which is ~455 $Å^3$. So the probe is about a fifth the size of AOT. In addition, its concentration in the bilayers is small, with 1 $W(CO)_6$ per 600 AOT. Therefore, the presence of $W(CO)_6$ should not have a significant influence on the global structure of the surfactant bilayers.

Figure 2 displays FT-IR absorption spectra of the asymmetric CO stretching mode of $W(CO)_6$ in AOT/water mixture with λ

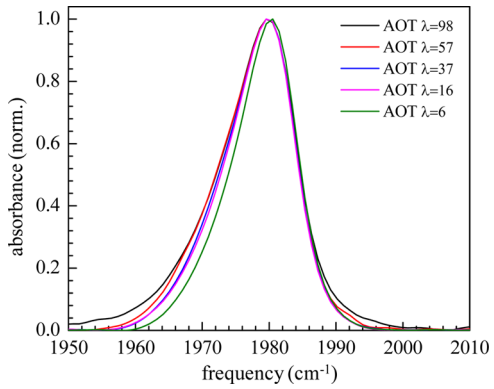

Figure 2. Background subtracted infrared absorbance spectrum of the CO stretching mode of tungsten hexacarbonyl ($W(CO)_6$) in AOT/water binary mixture with various water to surfactant ratios. λ = $[H_2O]/[AOT]$ = 98 to 16 are in the lamellar phase and λ = 6 is in the bicontinuous cubic phase.

(water molecules per AOT) ranging from 96 to 6. For λ = 96 to 16, the samples are lamellae, while for λ = 6, the sample is in the BC phase. The spectra with λ = 16 and 37 are identical. The spectra are not symmetrical. They have a steeper edge on the blue (high-frequency) side of the line than on the red side of the line. The λ = 57 and 98 samples appear to have increasingly longer tails on the red side of the lines. However, at these high water contents, there is a very large water background that must be subtracted out to obtain the spectra. It is possible that background subtraction errors at high water content give rise to

dx.doi.org/10.1021/ja312676e | J. Am. Chem. Soc. XXXX, XXX, XXX−XXX

the larger red tails. The λ = 6 (BC phase) spectrum is clearly narrower than the other spectra and its peak is shifted by ~0.5 cm^{-1} to the blue. The full widths at half-maximum (fwhm) from low to high water content are 11.02, 11.92, 12.27, 12.62, and 12.62 cm^{-1}.

$W(CO)_6$ is completely insoluble in water. Therefore, it resides in the hydrophobic interior of the lamellar and BC structures. Spectra can shed some light on the location of the vibrational probe within the lamellae and BC phase. Figure 3A shows the FT-IR absorption spectra of the CO asymmetric stretch of $W(CO)_6$ in the λ = 37 lamellae (red), dodecane (green), and EHS (the AOT model compound) (blue). The spectrum in the lamellae is clearly asymmetrical with steep rise on the blue side of the line and a broader red side. The peak of the spectrum in the lamellae falls between the other two peaks.

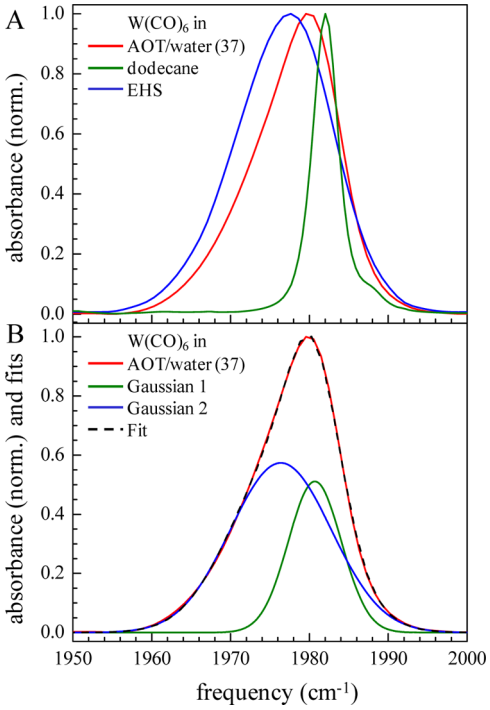

Figure 3. (A) Spectra of the CO stretching mode of $W(CO)_6$ in λ = 37 lamellae (red curve), in dodecane (green curve), and in EHS, the model liquid that is AOT without the sulfonate headgroup (see Figure 1). (B) The λ = 37 spectrum (red curve) and a two-Gaussian fit (black dashed curve). The two Gaussians that result from the fit are the blue and green curves. The blue Gaussian is virtually identical to the EHS spectrum shown in A. The green curve is slightly shifted and somewhat broader than the dodecane spectrum shown in A.

Figure 3B shows the spectrum in the lamellae (red) again with a fit (black dashed curve) to two Gaussians. The fit is basically perfect. The two Gaussians that compose the fit are also shown as the green and blue curves. The blue Gaussian in Figure 3B has parameters that are almost identical to a fit to the EHS spectrum in Figure 3A. The fit to the EHS data in Figure 3A yields a center position of 1976.9 cm^{-1} and a fwhm of 14.8 cm^{-1}. The blue Gaussian in Figure 3B has center position of 1976.4 cm^{-1} and a fwhm of 14.9 cm^{-1}. The fit to the dodecane data in Figure 3A yields a center position of 1982.0 cm^{-1} and a fwhm of 4.2 cm^{-1}. The green Gaussian in Figure 3B has center position of 1980.7 cm^{-1} and a fwhm of 7.6 cm^{-1}. The fit Gaussian is shifted somewhat to the red and is significantly broader than spectrum in dodecane.

As can be seen in Figure 3A, $W(CO)_6$ in dodecane has an exceedingly narrow line width of 4.2 cm^{-1} compared to its width in EHS (14.8 cm^{-1}). The line width in EHS is more typical. For example, the CO antisymmetric stretches of $W(CO)_6$ in CCl_4 and in $CHCl_3$ are 10 and 19 cm^{-1}, respectively.[50] Long linear hydrocarbons like dodecane tend to have all-trans configurations. The all-trans configuration will produce little variation in the local structure experienced by $W(CO)_6$, giving rise to the narrow line width. It is not unreasonable to assume that the branched alkane inside the lamellae is less ordered than in dodecane. Therefore, $W(CO)_6$ in the alkane region of AOT will have a wider the line width then it has in dodecane. The branching of the alkane portion of AOT and differences in packing are likely responsible for the somewhat increased width of Gaussian 1 (green curve) in the fit to the AOT spectrum shown in Figure 3B compared to the $W(CO)_6$ spectrum in dodecane. In EHS, $W(CO)_6$ can experience a wider range of environments giving rise to a broader line. In EHS, $W(CO)_6$ can be in an all alkane environment or it could be in contact with or near the ester moieties (see Figure 1). Given the spectrum in dodecane, presumably the blue side of the EHS line corresponds to more alkane-like environments and the on the red side of the line there are more interactions with the esters. It is important to note that $W(CO)_6$ does not have to come in direct contact with an ester oxygen to have its frequency shifted. As has been shown by comparison between experiments and simulations, frequency shifts that give rise to inhomogeneous broadening of vibrational absorption lines can arise from variations in the local electric field.[51−54]

The results of the fits in Figure 3B suggest that the $W(CO)_6$ experiences both alkane and ester environments but with the alkane environments dominating. Based on the molecular volume of EHS (392 $Å^3$) and the volume of the ester portion only (124 $Å^3$), EHS, (see Figure 1B) is very approximately composed of a one-third ester region and a two-thirds alkane region. The spectrum of $W(CO)_6$ in the pure alkane shows that the absorption is on the blue side of the peak of the spectrum in the lamellae. To fit the spectrum in the lamellae requires the EHS spectrum plus additional absorbance on the blue side of the line, indicating that the $W(CO)_6$ is exposed more to the alkane portion of the AOT than to the ester portion. Given the areas of the Gaussians in the fits in Figure 3B (ratio blue/green = 2.1) and the very approximate partitioning of the EHS into 33%/66% ester/alkane, a very crude estimate suggests that the $W(CO)_6$ is exposed to 77%/23% alkane/ester in the interior of the lamellae. This is one extreme. However, in EHS, $W(CO)_6$ will frequently be exposed to ester and alkane portions of the surrounding solvent simultaneously. If we take all of the EHS portion of the fit in Figure 3B (blue curve) to represent some interactions of $W(CO)_6$ with ester moieties and the green curve to represent interactions only with the alkane portions of AOT, then the ratio is 32%/68% alkane/ester. Here ester means some influence on $W(CO)_6$ because it is either in contact or near an ester. This is a wide range, but the results indicate that the ensemble of $W(CO)_6$ molecules is not located strictly in the alkane portion of the bilayers. It may be possible to obtain more detailed information on the $W(CO)_6$ environments through simulations.

$W(CO)_6$ is not polar. However, it is polarizable. Its polarizability will produce some attraction to the polar ester region of AOT. Returning to the spectra in Figure 2, the increasing tails to the red with increasing water content may

dx.doi.org/10.1021/ja312676e | J. Am. Chem. Soc. XXXX, XXX, XXX−XXX

indicate that the additional water, which penetrates to some extent into the ester regions of the AOT headgroup,[18] causes $W(CO)_6$ to partition to a greater extent into the ester region. Conversely, the fact the spectrum in the BC phase ($\lambda = 6$) has less spectral density to the red may indicate that in this phase, tungsten hexacarbonyl partitions less into the ester region of the AOT head groups.

3.2. Ultrafast IR Spectroscopy. To illustrate the nature of the data, 2D IR vibrational echo spectra of the asymmetric CO stretch of $W(CO)_6$ inside a lamellar structure ($\lambda = 24$) are shown in Figure 4 at two waiting times (T_w). The positive

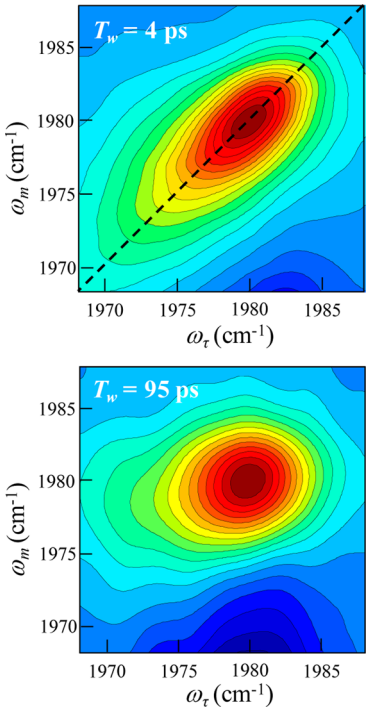

Figure 4. 2D IR vibrational echo spectra of the CO stretch of $W(CO)_6$ in $\lambda = 24$ lamellae. The top panel is at short time (T_w = 4 ps). It is substantially elongated along the diagonal (black dashed line). The bottom panel is at long time (T_w = 95 ps). The shape of the spectrum has changed substantially, and it has little elongation along the diagonal showing spectral diffusion is almost complete.

going bands (red) arise from the 0-1 vibrational transition. The negative going bands (blue), which are only partially shown below the 0-1 bands, arise from vibrational echo emission at the 1-2 vibrational frequency. These bands are shifted by the vibrational anharmonicity to lower frequency along the ω_m frequency axis. Changes are clearly visible in the 0-1 spectra. At early time (T_w = 4 ps, top panel), the spectrum is substantially elongated along the diagonal (black dashed line). The width perpendicular to the diagonal shows there is substantial homogeneous broadening of the absorption line. The elongation along the diagonal at short time arises because the line is inhomogeneously broadened and structural evolution of the system has not caused significant sampling at this short time of the range of inhomogeneous frequencies. At long time (T_w = 95 ps, bottom panel), the 2D IR spectrum is close to symmetrical, which shows that spectral diffusion is almost complete.

For each sample, 2D IR spectra are taken at many T_w values, and the change in shape with time is quantified with the CLS method.[47] The CLS data are presented in Figure 5. The data have important qualitative features. All of the AOT lamellar

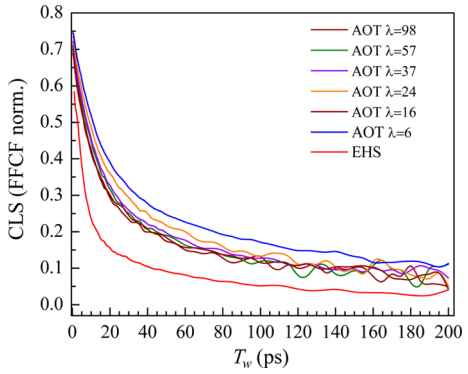

Figure 5. CLS curves for the CO stretching mode of $W(CO)_6$ in AOT/water binary mixtures in the lamellar phase, λ = 98 to 16, in the BC phase, $\lambda = 6$, and in the model liquid bis(2-ethylhexyl) succinate (EHS).

samples (λ = 98, 75, 37, 24, and 16) have almost identical decay curves. However, the AOT sample in the BC phase ($\lambda = 6$, blue curve) displays a significantly slower decay. In contrast, the data for $W(CO)_6$ in the EHS model liquid (red curve, AOT like structure but without the sulfonate, see Figure 2B) decay much faster than any of the other data. These results show that the dynamics interior to the lamellar structures have little dependence on the number of water molecules between the AOT bilayers. However, when the phase changes from lamellar to BC there is a change in dynamics. In addition, the decay curves show that the dynamics interior to the ordered phases are quite different from the dynamics in EHS liquid, which is a model of AOT without the sulfonate headgroup that causes AOT to form ordered phases in the presence of water.

The qualitative ideas are borne out by the quantitative analysis of the CLS curves that yield the FFCFs for each sample.[46,47] All of the CLS curves shown in Figure 5 are fit very well by a biexponential function. The difference between the T_w = 0 value of the CLS and 1 is related to the homogeneous component. Combining the CLS fit with the linear absorption spectrum makes it possible to calculate the full FFCF.[46,47] The FFCF parameters are given in Table 1. First, consider the lamellar samples, λ = 98 to 16. The slowest component of the decay of the FFCF is τ_2. All of the τ_2 values for the five lamellar samples are basically the same within experimental error. The average of the values is 147 ps. The faster components, τ_1, are also all the same within experimental error with an average for the five lamellar samples of 12.6 ps. The corresponding amplitude factors, Δ_1 and Δ_2, are also all the same within experimental error. Note that the deltas in Table 1 are the standard deviations. The total inhomogeneous line width is the convolution of these two Gaussians with standard deviation $(\Delta_1^2 + \Delta_2^2)^{1/2}$. The fwhm of the inhomogeneous line width is the total standard deviation multiplied by 2.35.

Table 1 also gives the homogeneous linewidths, Γ, and the corresponding homogeneous dephasing times, T_2. As with the spectral diffusion dynamics, the homogeneous dephasing is the same for the five lamellar samples (λ = 98 to 16) within experimental error. As discussed above, the homogeneous line width has contributions from pure dephasing, the vibrational lifetime, and the orientational relaxation (see eq 2). The vibrational lifetime (see Table 2) contributes only ~0.07 cm^{-1}

dx.doi.org/10.1021/ja312676e | J. Am. Chem. Soc. XXXX, XXX, XXX−XXX

Table 1. FFCF Parameters for the CO Stretching Mode of Tungsten Hexacarbonyl in AOT Lamellar Phase (λ = 98 to 16), in the Bicontinuous Cubic Phase (λ = 6), and in Bis(2-ethylhexyl) Succinate (EHS, AOT Model Liquid)

sample	T_2 (ps)	Γ (cm^{-1})	Δ_1 (cm^{-1})	τ_1 (ps)	Δ_2 (cm^{-1})	τ_2 (ps)
λ = 98	2.5 ± 0.2	4.3 ± 0.4	3.0 ± 0.2	12.0 ± 0.5	2.2 ± 0.4	149 ± 9
λ = 57	2.4 ± 0.2	4.4 ± 0.6	3.2 ± 0.4	13.4 ± 0.5	2.2 ± 0.6	154 ± 12
λ = 37	2.2 ± 0.4	4.9 ± 0.2	2.9 ± 0.6	12.5 ± 0.3	2.2 ± 0.6	144 ± 5
λ = 24	2.1 ± 0.3	5.0 ± 0.4	2.7 ± 0.5	13.4 ± 0.5	2.2 ± 0.4	139 ± 6
λ = 16	2.2 ± 0.2	4.9 ± 0.4	2.9 ± 0.3	11.7 ± 0.3	2.1 ± 0.3	149 ± 5
λ = 6	2.5 ± 0.2	4.1 ± 0.5	2.8 ± 0.2	14.7 ± 0.4	2.3 ± 0.5	178 ± 4
EHS	1.3 ± 0.3	8.2 ± 0.4	4.4 ± 0.2	4.8 ± 0.3	2.4 ± 0.4	80 ± 9

Table 2. Vibrational Lifetimes ($P(t)$) and Orientational Decay Times (τ_r) for the CO Stretching Mode of Tungsten Hexacarbonyl in AOT Lamellar Phase (λ = 98 to 16), in the Bicontinuous Cubic Phase (λ = 6), and in Bis(2-ethylhexyl) Succinate (EHS, AOT Model Liquid)

sample	$P(t)$ (ps)	τ_r (ps)
λ = 98	69 ± 0.6	4.0 ± 0.3
λ = 57	73 ± 0.3	4.7 ± 0.4
λ = 37	74 ± 0.3	3.7 ± 0.3
λ = 24	80 ± 0.5	4.0 ± 0.1
λ = 16	85 ± 0.3	4.5 ± 0.1
λ = 6	88 ± 0.3	3.4 ± 0.2
EHS	86.0 ± 0.8	3.9 ± 0.1

to the homogeneous line width. Orientational relaxation contributes ~0.9 cm^{-1}. Therefore, the homogeneous line width is dominated by pure dephasing, which results from ultrafast motions that produce a motionally narrowed component of the total absorption line width.

When the phase changes, the dynamics change. In the BC phase (λ = 6), the spectral diffusion is slower. The slow component τ_2 = 178 ± 4 ps, in contrast to the average of 147 ps for the lamellar phase samples. The fast component τ_1 = 14.7 ± 0.4 ps, in contrast to the average of 12.6 ps for the lamellar phase samples. Therefore, both components of the spectral diffusion are slower in the BC phase.

The water at the surface of AOT lamellae and at the AOT surface of large reverse micelles undergoes orientational relaxation in 18 ps.[18,38,39] The water in reverse micelles undergoes slower orientational relaxation as the number of water molecules per AOT decreases.[39] For 10 waters per headgroup it is 26 ps, and for 5 waters, it is 30 ps.[39] Given these results, it is likely that the water orientational relaxation in the BC phase with λ = 6 is somewhat slower than the 18 ps orientational relaxation of water at the surfaces of the lamellae. These water orientational relaxation times are much faster than the slow components of the spectral diffusion in either the lamellar or BC phases, although they are comparable to the fast components. It is unlikely that the water dynamics play a significant role in the spectral diffusion measured inside of the surfactant structures, although it cannot be ruled out for the fast component. Therefore, it is reasonable to assume that the slowing of structural dynamics in the BC phase results from the difference in geometry of the BC phase compared to the lamellar phase rather than from the reduction in the number of water molecule per AOT per se. The organization of the AOT in the BC phase is different than it is in the lamellar phase. The difference in the physical arrangement of the surfactant molecules in the two phases results in a difference in the rates of structural dynamics.

While going from the lamellar phase to the BC phase causes a modest slowing of the structural dynamics, the dynamics in the EHS model liquid (see Figure 1) are substantially different. The CO mode of $W(CO)_6$ in EHS has τ_2 = 80 ± 9 ps and τ_1 = 4.8 ± 0.3 ps. These times are almost factors of two and three times faster, respectively, than the corresponding times in the ordered phases. In addition, the homogeneous line width in EHS is almost a factor of 2 wider than it is in the ordered phases. EHS is a normal liquid with no long-range ordering in its structure. Given the disorder, $W(CO)_6$ should be in proximity to both the alkane and ester portions of the EHS molecule. It was argued in connection with the FT-IR spectra in Figures 2 and 3 that the absorption spectra of the asymmetric CO stretch of $W(CO)_6$ in the AOT/water ordered phases is similar to that in EHS but with more contribution from the alkane-like spectrum in the AOT/water samples.

The spectral diffusion dynamics as well as the pure dephasing dynamics are very different in the ordered lamellar and BC phases than they are in the EHS model liquid (see Table 1) even though the chemical nature of the environments in the ordered and disordered systems are very similar. These results demonstrate that the organization of the interiors of lamellae and BC structures have a substantial influence on the structural dynamics. Going from one ordered phase to another, lamellar to BC, has some effect on dynamics. While in the lamellar phase, the structures are planar, in the BC phase, the dominant structure is more akin to cylinders. This change will affect the packing of the AOT hydrocarbon tails in the interior of the ordered structures, which evidently has an impact on the structural dynamics. However, the change from one ordered structure to another has a small influence on dynamics compared to the effect of order vs disorder.

In both the ordered phases and the disordered liquid, there are two time scales for the spectral diffusion that are more than an order of magnitude different. The FFCF is described in terms of a multiexponential model. The time constants, τ_1 and τ_2 given in Table 1 should be thought of as time scales for processes rather than time constants for specific processes as there may be a collection of motions, which occur with about the same rates, that give rise to the time constants obtained from the fits. The time scales may reflect motions of the side chains (fast) and motions of the total AOT or EHS molecules (slow), with the disordered EHS liquid having overall faster motions of both types. Regardless of the exact nature of the motions, it is clear that the order imposed by lamellar and BC phases substantially slows the structural dynamics.

Although the amount of water between the lamellae layers does not influence the structural dynamics as reported by the spectral diffusion within experimental error, there is evidence that there may be minor changes in the local environment of $W(CO)_6$ with water content. Figure 6 shows the results of

dx.doi.org/10.1021/ja312676e | J. Am. Chem. Soc. XXXX, XXX, XXX−XXX

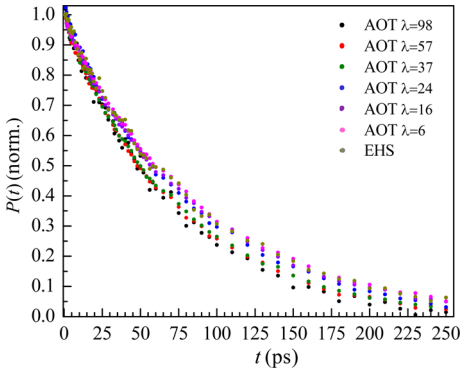

Figure 6. Magic angle pump–probe data (lifetimes) for the CO stretch of $W(CO)_6$ in the AOT/water lamellar phase (λ = 98, 57, 37, 24, 16), in the bicontinuous cubic phase (λ = 6), and in the model liquid bis(2-ethylhexyl) succinate (EHS).

pump–probe data taken at the magic angle for all of the samples. These decays are the vibrational lifetimes, $P(t)$ (see eqs 3 and 4). The vibrational lifetime is very sensitive to the very local environment and intermolecular interactions. This is in contrast to spectral diffusion that is caused by global structural reorganization of a system. In a number of systems, such as proteins,[51−53] water,[55,56] and water/salt solutions,[57] the influence of structural fluctuations on a vibrational frequency has been modeled in terms of fluctuating electric fields. Global motions of the environment cause the electric field along the vibrational transition dipole direction to fluctuate, which via the Stark effect, gives rise to time dependent frequency fluctuations.[51]

All of the decays in Figure 6 fit extremely well to single-exponential functions. The results of the fits are given in Table 2. As the number of water molecules per AOT decreases from 98 to 6, the vibrational lifetime increases from 69 to 88 ps. Because the decays are single exponential and can be measured over several lifetimes, the error bars are small (see Table 2). The progression of the lifetimes indicates local structural change with water content. Either these changes do no influence the structural dynamics of the systems or the influence is too small to be picked up in the measurements of spectral diffusion. Note that while going from the lamellar phase to the BC phase causes a jump in both the fast and slow spectral diffusion time constants, the changes in the lifetimes seems to progress smoothly without a noticeable discontinuity when the phase changes.

Combining the pump–probe magic angle and parallel polarization experiments, the $W(CO)_6$ transition dipole orientational anisotropy decays were measured (see eqs 3 and 4). The results are given in Table 2. All of the anisotropy decays are virtually the same. The anisotropy decay of the asymmetric CO stretch of $W(CO)_6$ is not caused by normal molecular reorientation. The CO stretch is triply degenerate. The excitation pulse projects out a superposition of the three modes that results in the initially excited transition dipole being along the pump pulse electric field.[58] Then fluctuations that cause this initial superposition to change result in a change in the direction of the transition dipole without physical reorientation of the molecule.[58] Therefore, the anisotropy decays in these systems do not provide the type of information that normal orientational relaxation measurements do and cannot be interpreted in terms of shape factors, hydrodynamic boundary conditions, or friction coefficients.

In all of the systems, the anisotropy decay is faster than either of the spectral diffusion time constants. It is important to recognize that the anisotropy relaxation correlation function, the second Legendre polynomial correlation function, obtained from the pump–probe experiments is a different correlation function than the FFCF. Therefore, the resulting time constants cannot be directly compared. As an example, for Gaussian fluctuation anisotropy relaxation that is single exponential, dielectric relaxation, which measures the first Legendre polynomial correlation function, gives a time constant that is three times as long as that which would be measured by a pump–probe experiment on the same system.[59,60]

4. CONCLUDING REMARKS

Surfactant bilayers occur very commonly in systems such as vesicles and cell membranes. Here we have examined the dynamics inside surfactant bilayers, which are important for processes that involve bilayers. Molecules can pass through the walls of vesicles and cell membranes. Such transmission of molecules through a bilayer involves the structural fluctuations of the bilayer interior. Cell membranes contain a wide array of transmembrane proteins. For transmembrane proteins, the bilayer is the "solvent" in which biological processes occur. Chemistry depends to a great extent on the nature of the solvent, which provides dynamical intermolecular interactions that are intimately involved in chemical processes. For cytosolic proteins and enzymes, the water medium matters. MD simulations use sophisticated water models that do a reasonable job of reproducing the mechanical degrees of freedom of water. Even when implicit water models are used, these are tweaked to mimic atomistic water models. The bath degrees of freedom can be included in MD simulations of cytosolic proteins and enzymes because we have an extensive understanding of water dynamics, and water simulations have been tested against experiments, principally ultrafast 2D IR vibrational echo experiments.[61−64] The equivalent detailed simulations based on 2D IR experimental information that is available for water[61,62] are not available for the interiors of surfactant bilayers. The results presented here are an initial step in increasing our understanding of the structural dynamics of surfactant bilayers.

The results presented above provide the first detailed examination of the fast structural dynamics of the interior of surfactant bilayers in both the lamellar phase and the bicontinuous cubic phase. For the lamellae, multibilayers with 16–98 water molecules per AOT surfactant molecule were studied and it was determined that the thickness of the water layer that separates bilayers does not influence the internal structural dynamics of the bilayers. Sixteen water molecules are sufficient to solvate the AOT headgroup and its sodium counterion.[18] As the number of water molecules per AOT is increased, the water layer away from the bilayer/water interface becomes increasingly bulk-like. By 98 water molecules per AOT, there is a substantial bulk-like slab of water between the bilayers. The results show that an increased separation of the bilayers by bulk-like water does not change the internal structural dynamics.

Changing the phase does change the dynamics to a small but measurable extent. A reduction in the number of water molecules per AOT to six causes a phase change to BC. The internal structural dynamics in the BC phase are ~20% slower than in the lamellar phase. However, the dynamics in both the lamellar and BC phases are much slower than those of the

dx.doi.org/10.1021/ja312676e | J. Am. Chem. Soc. XXXX, XXX, XXX–XXX

model liquid, bis(2-ethylhexyl) succinate (EHS), which is identical to AOT except that it lacks the charged sulfonate headgroup (see Figure 1). Without the sulfonate head groups interacting with water, EHS does not form ordered structural phases. It is essentially identical chemically to the interior of the AOT bilayers but without the ordered structure. In EHS the fast and slow time scale dynamics are approximately factors of 3 and 2 faster, respectively, than the corresponding dynamics in the AOT ordered phases. Thus the order imposed by the interaction of the charged head groups with water has a very substantial impact on the internal structural dynamics of the lamellar and BC phases.

The results provided here are a test bed for MD simulations of the internal structural dynamics of the AOT bilayers. MD simulations of systems such as water[61,62] and proteins[52−54,65] have been compared to 2D IR vibrational echo experimental determinations of frequency−frequency correlation functions. The time scales of the measured dynamics, tens to hundreds of picoseconds are readily amenable to MD simulations. Reasonable reproduction of the 2D IR results by simulations validates the simulations, which then permits the use of the simulations to associate specific molecular motions with the measured time scales.

The experiments on AOT are a first step in understanding the fast internal structural dynamics of multibilayers. The experiments used here on AOT systems are currently being extended to the study of phospholipid multibilayer models of cell membranes.

AUTHOR INFORMATION

Corresponding Author

fayer@stanford.edu

Notes

The authors declare no competing financial interest.

ACKNOWLEDGMENTS

This work was funded by the Division of Chemical Sciences, Geosciences, and Biosciences, Office of Basic Energy Sciences of the U.S. Department of Energy through Grant No. DE-FG03-84ER13251. We thank Aanindeeta Banerjee for help with the synthesis of EHS. A.T. thanks the Stanford Graduate Fellowship program for a research fellowship.

REFERENCES

(1) Petrov, P. G.; Ahir, S. V.; Terentjev, E. M. *Langmuir* **2002**, *18*, 9133−9139.
(2) Garza, C.; Thieghi, L. T.; Castillo, R. *J. Chem. Phys.* **2007**, *126*, 051106−051105.
(3) Fontell, K. *J. Colloid Interface Sci.* **1973**, *44*, 318−329.
(4) Metzler, D. E. *Biochemistry: The Chemical Reactions of Living Cells*, 2nd ed.; Harcourt/Academic Press: San Diego, 2001.
(5) Milhaud, J. *Biochim. Biophys. Acta* **2004**, *1663*, 19−51.
(6) Zhao, W.; Moilanen, D. E.; Fenn, E. E.; Fayer, M. D. *J. Am. Chem. Soc.* **2008**, *130*, 13927−13937.
(7) Monnoyer, P.; Fonseca, A.; Nagy, J. B. *Colloids Surf., A-Physicochem. Eng. Aspects* **1995**, *100*, 233−243.
(8) Johansson, K. P.; Marchetti, A. P.; McLendon, G. L. *J. Phys. Chem.* **1992**, *96*, 2873−2879.
(9) Janmey, P. A.; Kinnunen, P. K. J. *Trends Cell Biol.* **2006**, *16*, 538−546.
(10) Bienveniie, M.; Marie, J. S. *Curr. Top. Membr.* **1994**, *40*, 319−354.
(11) Jensen, M. O.; Mouritsen, O. G. *Biochim. Biophys. Acta-Biomembr.* **2004**, *1666*, 205−226.
(12) Mcintosh, T. J.; Simon, S. A. *Annu. Rev. Biophys. Biomol.* **2006**, *35*, 177−198.
(13) Lee, A. G. *Biochim. Biophys. Acta-Rev. Biomembr.* **2004**, *1666*, 62−87.
(14) Gradzielski, M.; Hoffmann, H.; Panitz, J.-C.; Wokaun, A. *J. Colloid Interface Sci.* **1995**, *169*, 103−118.
(15) Neto, A. M. F.; Salinas, S. R. A. *The Physics of Lyotropic Liquid Crystals*; Oxford University Press: New York, 2005.
(16) Boissiere, C.; Brubach, J. B.; Mermet, A.; de Marzi, G.; Bourgaux, C.; Prouzet, E.; Roy, P. *J. Phys. Chem. B* **2002**, *106*, 1032−1035.
(17) Nallet, F.; Laversanne, R.; Roux, D. *J. Phys. II Fr.* **1993**, *3*, 487−502.
(18) Moilanen, D. E.; Fenn, E. E.; Wong, D.; Fayer, M. D. *J. Am. Chem. Soc.* **2009**, *131*, 8318−8328.
(19) Lopez, C. F.; Nielsen, S. O.; Klein, M. L.; Moore, P. B. *J. Phys. Chem. B* **2004**, *108*, 6603−6610.
(20) Disalvo, E. A.; Lairion, F.; Martini, F.; Tymczyszyn, E.; Frias, M.; Almaleck, H.; Gordillo, G. J. *Biochim. Biophys. Acta-Biomembr.* **2008**, *1778*, 2655−2670.
(21) Bhide, S. Y.; Berkowitz, M. L. *J. Chem. Phys.* **2006**, *125*, 094713.
(22) Eicke, H.-F.; Rehak, J. *Helv. Chim. Acta* **1976**, *59*, 2883−2891.
(23) Nagle, J. F.; Tristram-Nagle, S. *Biochim. Biophys. Acta-Rev. Biomembr.* **2000**, *1469*, 159−195.
(24) Tristram-Nagle, S.; Nagle, J. F. *Chem. Phys. Lipids* **2004**, *127*, 3−14.
(25) Hubner, W.; Blume, A. *Chem. Phys. Lipids* **1998**, *96*, 99−123.
(26) Gawrisch, K.; Gaede, H. C.; Mihailescu, M.; White, S. H. *Eur. Biophys. J. Biophys. Lett.* **2007**, *36*, 281−291.
(27) Khandelia, H.; Kaznessis, Y. N. *Biochim. Biophys. Acta-Rev. Biomembr.* **2007**, *1768*, 509−520.
(28) Damodaran, K. V.; Merz, J., K. M. *Langmuir* **1993**, *9*, 1179−1183.
(29) Hubbard, P. L.; McGrath, K. M.; Callaghan, P. T. *J. Phys. Chem. B* **2006**, *110*, 20781−20788.
(30) Callaghan, P. T.; Soderman, O. *J. Phys. Chem.* **1983**, *87*, 1737−1744.
(31) Aslund, I.; Cabaleiro-Lago, C.; Soderman, O.; Topgaard, D. *J. Phys. Chem. B* **2008**, *112*, 2782−2794.
(32) Verma, P. K.; Saha, R.; Mitra, R. K.; Pal, S. K. *Soft Matter* **2010**, *6*, 5971−5979.
(33) Lesslauer, W.; Cain, J. E.; Blasie, J. K. *Proc. Natl. Acad. Sci. U.S.A.* **1972**, *69*, 1499−1503.
(34) Krishnamoorthy, G. *J. Phys. Chem. B* **2001**, *105*, 1484−1488.
(35) Aguilar, L. F.; Pino, J. A.; Soto-Arriaza, M. A.; Cuevas, F. J.; Sánchez, S.; Sotomayor, C. P. *PLoS ONE* **2012**, *7*, e40254.
(36) Zannoni, C.; Arcioni, A.; Cavatorta, P. *Chem. Phys. Lipids* **1983**, *32*, 179−250.
(37) Podo, F.; Blasie, J. K. *Proc. Natl. Acad. Sci. U.S.A.* **1977**, *74*, 1032−1036.
(38) Moilanen, D. E.; Fenn, E. E.; Wong, D.; Fayer, M. D. *J. Phys. Chem. B* **2009**, *113*, 8560−8568.
(39) Moilanen, D. E.; Fenn, E. E.; Wong, D.; Fayer, M. D. *J. Chem. Phys.* **2009**, *131*, 014704.
(40) Moilanen, D. E.; Levinger, N.; Spry, D. B.; Fayer, M. D. *J. Am. Chem. Soc.* **2007**, *129*, 14311−14318.
(41) Fenn, E. E.; Wong, D. B.; Fayer, M. D. *Proc. Natl. Acad. Sci. U.S.A.* **2009**, *106*, 15243−15248.
(42) Fenn, E. E.; Wong, D. B.; Fayer, M. D. *J. Chem. Phys.* **2011**, *134*, 054512.
(43) Mukamel, S. *Principles of Nonlinear Optical Spectroscopy*; Oxford University Press: New York, 1995.
(44) Mukamel, S. *Annu. Rev. Phys. Chem.* **2000**, *51*, 691−729.
(45) Park, S.; Kwak, K.; Fayer, M. D. *Laser Phys. Lett.* **2007**, *4*, 704−718.
(46) Kwak, K.; Park, S.; Finkelstein, I. J.; Fayer, M. D. *J. Chem. Phys.* **2007**, *127*, 124503.
(47) Kwak, K.; Rosenfeld, D. E.; Fayer, M. D. *J. Chem. Phys.* **2008**, *128*, 204505.

(48) Gold, S.; Eastoe, J.; Grilli, R.; Steytler, D. C. *Colloid Polym. Sci.* **2006**, *284*, 1333−1337.
(49) Kumar, S. K. K.; Tamimi, A.; Fayer, M. D. *J. Chem. Phys.* **2012**, *137*, 184201.
(50) Tokmakoff, A.; Sauter, B.; Fayer, M. D. *J. Chem. Phys.* **1994**, *100*, 9035−9043.
(51) Williams, R. B.; Loring, R. F.; Fayer, M. D. *J. Phys. Chem. B* **2001**, *105*, 4068−4071.
(52) Merchant, K. A.; Noid, W. G.; Akiyama, R.; Finkelstein, I.; Goun, A.; McClain, B. L.; Loring, R. F.; Fayer, M. D. *J. Am. Chem. Soc.* **2003**, *125*, 13804−13818.
(53) Bagchi, S.; Nebgen, B. T.; Loring, R. F.; Fayer, M. D. *J. Am. Chem. Soc.* **2010**, *132*, 18367−18376.
(54) Bagchi, S.; Boxer, S. G.; Fayer, M. D. *J. Phys. Chem. B* **2012**, *116*, 4034−4042.
(55) Eaves, J. D.; Tokmakoff, A.; Geissler, P. L. *J. Phys. Chem. A* **2005**, *109*, 9424−9436.
(56) Corcelli, S. A.; Lawrence, C. P.; Asbury, J. B.; Steinel, T.; Fayer, M. D.; Skinner, J. L. *J. Chem. Phys.* **2004**, *121*, 8897−8900.
(57) Lin, Y.-S.; Auer, B. M.; Skinner, J. L. *J. Chem. Phys.* **2009**, *131*, 144511.
(58) Tokmakoff, A.; Urdahl, R. S.; Zimdars, D.; Francis, R. S.; Kwok, A. S.; Fayer, M. D. *J. Chem. Phys.* **1995**, *102*, 3919−3931.
(59) Gaffney, K. J.; Piletic, I. R.; Fayer, M. D. *J. Chem. Phys.* **2003**, *118*, 2270−2278.
(60) Berne, B. J.; Pecora, R. *Dynamic Light Scattering*; J. Wiley: New York, 1976.
(61) Asbury, J. B.; Steinel, T.; Kwak, K.; Corcelli, S. A.; Lawrence, C. P.; Skinner, J. L.; Fayer, M. D. *J. Chem. Phys.* **2004**, *121*, 12431−12446.
(62) Asbury, J. B.; Steinel, T.; Stromberg, C.; Corcelli, S. A.; Lawrence, C. P.; Skinner, J. L.; Fayer, M. D. *J. Phys. Chem. A* **2004**, *108*, 1107−1119.
(63) Fecko, C. J.; Eaves, J. D.; Loparo, J. J.; Tokmakoff, A.; Geissler, P. L. *Science* **2003**, *301*, 1698−1702.
(64) Fecko, C. J.; Loparo, J. J.; Roberts, S. T.; Tokmakoff, A. *J. Chem. Phys.* **2005**, *122*, 054506−054518.
(65) Merchant, K. A.; Noid, W. G.; Thompson, D. E.; Akiyama, R.; Loring, R. F.; Fayer, M. D. *J. Phys. Chem. B* **2003**, *107*, 4−7.